International Journal of Modern Manufacturing Technologies
ISSN 2067–3604, Vol. XVII, No. 1 / 2025
https://doi.org/ 10.54684/ijmmt.2025.17.1.70

OPTIMIZATION OF SURFACE ROUGHNESS IN TURNING USING STATISTICAL ANALYSIS AND MACHINE LEARNING

Razali Samin[1], Luqman Hakim Noorazlan[2], Mohd Idris Shah Ismail [3], Mohd Hafis Sulaiman[4]

[1-4]Universiti Putra Malaysia, Department of Mechanical and Manufacturing Engineering
Faculty of Engineering, Universiti Putra Malaysia, 43400 UPM, Serdang, Selangor, Malaysia

Corresponding author: Razali Samin, zali@upm.edu.my

Abstract: Surface roughness optimization plays a crucial role in ensuring the quality and cost-efficiency of machined products. This work uses machine learning and Response Surface Methodology (RSM) to predict and optimize surface roughness during mild steel CNC turning. Crucial process variables like cutting speed, feed rate, and depth of cut were investigated in order to develop accurate prediction models. Surface roughness (*Ra*, *Rq*, *Rz*) and cutting forces were recorded using a Mitutoyo SJ-210 and a Kistler 9257B dynamometer, respectively. Experiments were performed under varied conditions, and both statistical analysis and machine learning techniques were employed. Optimal machining parameters were identified as 300 m/min cutting speed, 0.15 mm/rev feed rate, and 0.5 mm depth of cut. The RSM and artificial neural network (ANN) models showed high prediction accuracy, with ANN achieving an R-value of 0.9943. The findings confirm the effectiveness of combining statistical and machine learning methods for surface quality improvement in CNC turning.
Key words: turning, statistical analysis, machine learning, surface roughness, cutting force

1. INTRODUCTION

The surface roughness, tool wear, material removal rate, and tool life of a turning process are significantly influenced by cutting speed, lubrication, feed rate, depth of cut, and numerous other input variables. Measured in *Ra* or *Rz*, surface roughness is critical since it directly affects a component's performance and longevity. Poor surfaces, or abruptions, are commonly considered the root cause of failure in an engineered part. The turning operation is a typical manufacturing process using a single point cutting tool to remove material from a cylindrical workpiece. There are numerous methods for calculating machine performance, but the most prevalent practice is to compute the surface roughness of various materials. For optimal results, different types and values of specific parameters are considered.

In recent years, Liu et al. (2019) proposed radial ultrasonic vibration-assisted turning to create micro-textured surfaces at low cost and in high volume. The consistency between the theoretical model and the outcomes of the simulations and experiments demonstrates that surfaces covered with uniformly spaced micro-dimples can be manufactured. Processing parameters such as clearance angle, spindle speed, feed rate, and vibration amplitude strongly affect micro-dimple organisation and shape.

On top of that, Veeranaath et al. (2022) believed that ANN is a solid modelling approach in which ANN models can persistently store, forward, and interpret the information specified and predict data that has yet to be provided. The model is a straightforward approximation of the human brain. Neurons are accumulated to create the ANN. This stacking up occurs in layers and is not random. The ANN's three primary layers comprise the input, hidden, and output layers. The first layer's objects relay upcoming data from the external biosphere to the hidden second layer. Unlike the second layer, information in the first does not get as much dispersal. In the buried layer, information from brain cells in the previous layer's factors and their summary and initiation functions shape responses.

Moreover, Santhosh et al. (2021) also affirmed that the typical architectures for modelling Artificial Neural Networks consist of an input layer, a hidden layer, and an output layer. The input layer manages process factors such as feed rate, rotating speed, and cut depth. Afterwards, to increase the accuracy of the output value, the hidden layer should be programmed with the appropriate number of neurons. This project applies machine learning and statistical approaches to modelling and optimising surface roughness in machining. As machining processes rely on many parameters that affect the final product quality, the statistical approach is vital to a deeper understanding of the relationship between parameters, and which parameter is significant compared to others. Meanwhile, ML allows the data obtained in the experiment to be analysed, generating more robust predictions.

2. METHODOLOGY

2.1 Material and methods

The experiment used an S45C medium carbon steel workpiece with a hardness of 59 HRB. The steel, with its nominal material composition, was used in the form of a round bar measuring 75 mm in diameter and 250 mm in length. The cutting parameters examined included cutting speed, with the selected ranges based on the recommendations provided by the cutting tool manufacturer, as shown in Table 1. The cutting force was measured during the turning operation in the feed direction (*Fz*), tangential (to the rotation of the workpiece) direction (*Fy*) and the radial or thrust directions (*Fx*) on a dynamometer installed to the tool holder as shown in Figure 1.

Table 1. Parameters for cutting conditions

Parameters	Min	Max
f (mm/rev)	0.15	0.25
d (mm)	0.5	2.5
Vs (m/min)	50	300

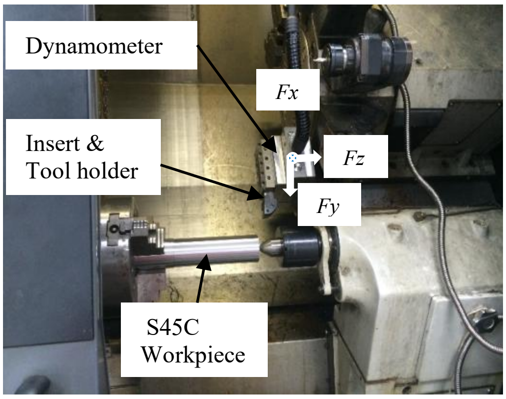

Fig. 1. Experimental setup with dynamometer

This experiment was conducted using a CNC turning machine (Mazak 200MY) with a maximum spindle speed of 20,000 rpm, controlled by the PC-Fusion-CNC system (Mazatrol 640T). A CVD-coated carbide insert (Sumitomo AC2000 CNMG120404N-GU) was used for turning operations under dry-cutting conditions. The ISO-certified tool holder (ECLNR-2020K12, Chain Carbide) was used to mount the insert. Using a Kistler 9129AA dynamometer, cutting forces were determined. A data collection system (model 5697A) was interfaced with an amplifier (type 5070A, 4-channel) that was attached to the dynamometer. DAQ software (version 2.6.5.16) and Dynoware software (model 2825D-02) were used to record cutting force signals. A portable MarSurf Psi gauge was used to measure the machined workpiece's surface roughness.

2.2. Statistical and machine learning approaches

The methodology combines machine learning and statistical approaches to model and optimize surface roughness in machining processes. The objective is to develop accurate predictive models and effective optimization strategies to improve surface quality. Supervised machine learning methods were employed to model the relationship between machining parameters and surface roughness. In parallel, statistical techniques were used to analyze and model the surface roughness data. The statistical analysis program's tools were utilized. The primary factors influencing surface roughness were identified and measured using Response Surface Methodology (RSM) in Design Expert software. Analysis of variance (ANOVA) was also used to validate statistical models and assess their reliability. Choosing important machining parameters, such as feed rate, depth of cut, and cutting speed, was part of the data collection process. Cutting forces were measured to capture the dynamics of the machining process, while surface roughness data was collected using profilometers.
Then, the developed models were trained and validated using the data collected by MATLAB software for modelling and neural network analysis programs. Model accuracy and predictability were evaluated using performance metrics such as mean squared error (MSE) and R-squared (R^2). Optimization techniques were then integrated with the models to identify the optimal machining parameters for achieving the desired surface

roughness. The optimal settings were determined by systematically exploring the parameter space using RSM. Finally, the models and optimization outcomes were validated by comparing them with existing empirical models or through experimental verification using physical machining tests.

3. RESULTS AND DISCUSSION

3.1. Cutting forces and surface roughness values

In this paper, the results as stated in Table 2 shows the cutting parameters for 20 runs and surface roughness value measurements. Figures 2 through 21 show the measured cutting force values for runs 1 through 20. The S45C tool insert with CBN is turned under a dry cutting machine at various cutting settings. Three force measurement directions are transmitted by the stationary dynamometer: cutting or tangential force (*Fy*), feed or axial force (*Fx*), and radial or thrust force (*Fz*).

Table 2. Cutting parameters and surface roughess values

Run	*Vs* (m/min)	*f* (mm/rev)	*d* (mm)	*Ra* (μm)	*Rq* (μm)	*Rz* (μm)
1	50	0.25	0.5	7.8613	9.4855	37.7525
2	50	0.25	2.0	8.0115	9.6383	38.2535
3	50	0.15	0.50	5.1078	6.3002	29.3300
4	50	0.15	2.00	3.8656	5.1322	22.0984
5	175	0.20	2.00	5.1062	6.1122	24.8578
6	175	0.25	1.25	6.0310	7.1580	27.3346
7	175	0.20	0.50	3.6550	4.4152	18.4624
8	175	0.15	1.25	3.5722	4.3466	18.8168
9	175	0.20	1.25	4.8006	5.7986	24.0186
10	175	0.25	1.25	7.0096	8.4160	33.5488
11	175	0.20	1.25	4.9476	5.9144	24.0596
12	175	0.15	1.25	3.4124	4.0804	16.6988
13	300	0.15	0.50	2.5734	3.1730	14.5080
14	300	0.20	1.25	3.8646	4.6378	18.9078
15	300	0.25	2.00	5.8780	7.2028	30.7126
16	300	0.15	2.00	2.6372	3.1456	13.0764
17	300	0.25	0.50	5.8610	6.9096	26.9238
18	175	0.20	1.25	4.3512	5.2092	20.7680
19	175	0.20	1.25	4.8990	5.7814	23.3412
20	50	0.20	1.25	5.1414	6.3098	27.0504

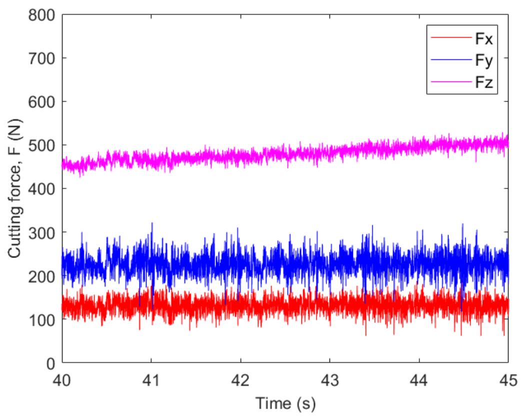

Fig. 2. Variation of the shear forces for:

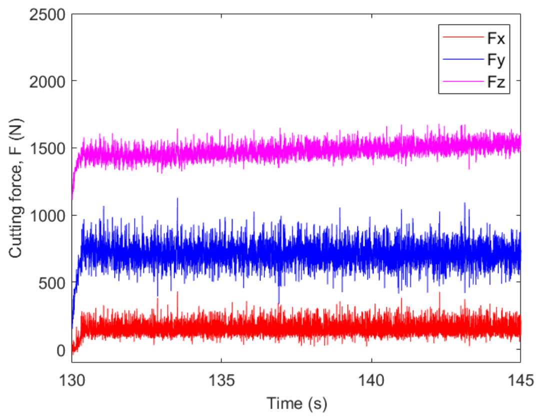

Fig. 3. Variation of the shear forces for:

Vs = 50 m/min, *d* = 0.5 mm, *f* = 0.25 mm/rev

Vs = 50 m/min, *d* = 2 mm, *f* = 0.25 mm/rev

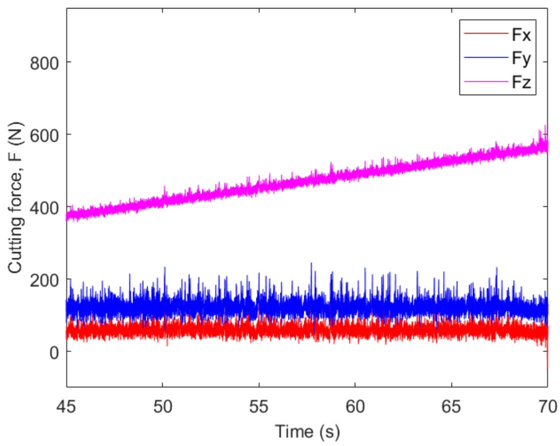

Fig. 4. Variation of the shear forces for:
Vs = 50 m/min, *d* = 0.5 mm, *f* = 1.5 mm/rev

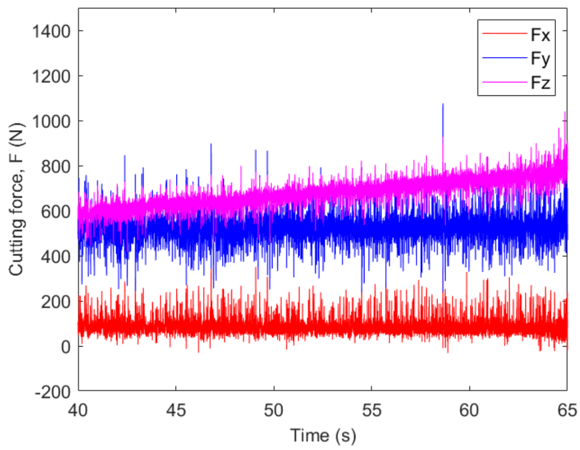

Fig. 5. Variation of the shear forces for:
Vs = 50 m/min, *d* = 2 mm, *f* = 0.5 mm/rev

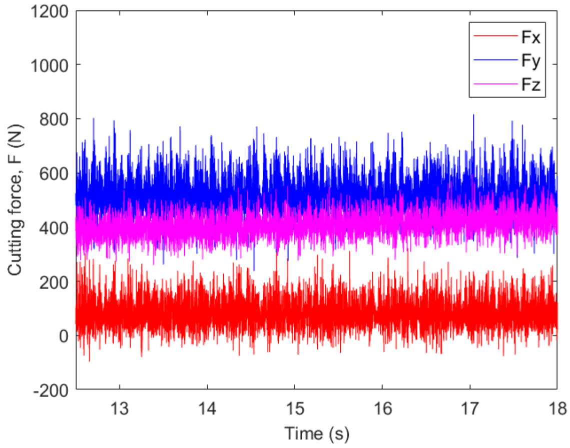

Fig. 6. Variation of the shear forces for:
Vs = 175 m/min, *d* = 2 mm, *f* = 0.2 mm/rev

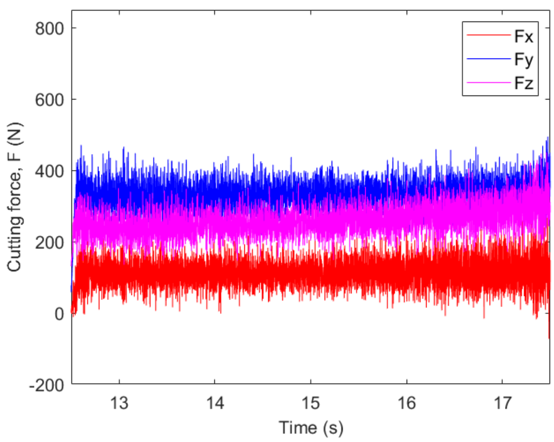

Fig. 7. Variation of the shear forces for:
Vs = 175 m/min, *d* = 1.25 mm, *f* = 0.25 mm/rev

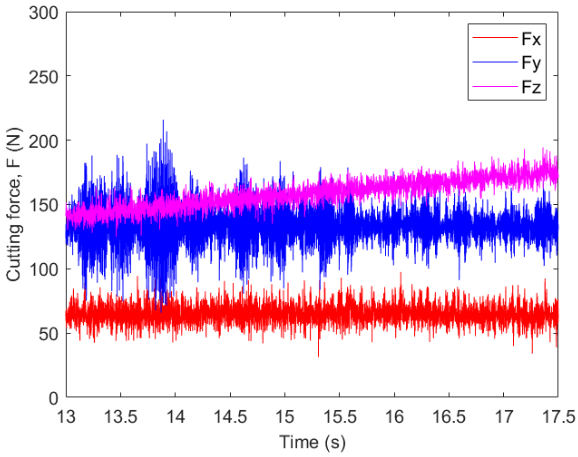

Fig. 8. Variation of the shear forces for:
Vs = 175 m/min, *d* = 0.5 mm, *f* = 0.2 mm/rev

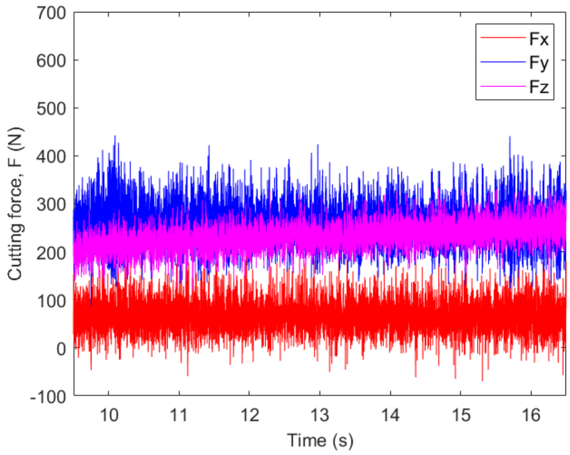

Fig. 9. Variation of the shear forces for:
Vs = 175 m/min, *d* = 1.25 mm, *f* = 0.15 mm/rev

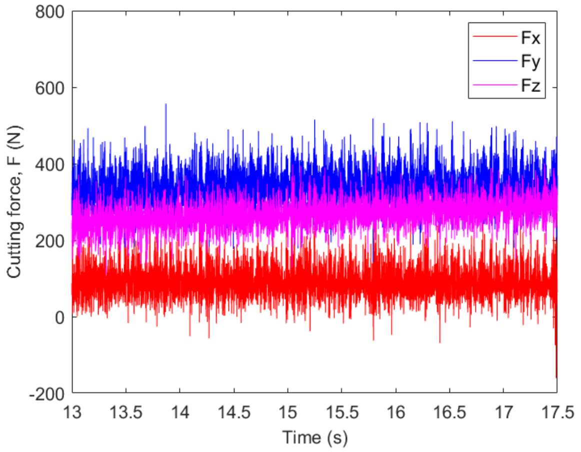

Fig. 10. Variation of the shear forces for:
Vs = 175 m/min, *d* = 1.25 mm, *f* = 0.2 mm/rev

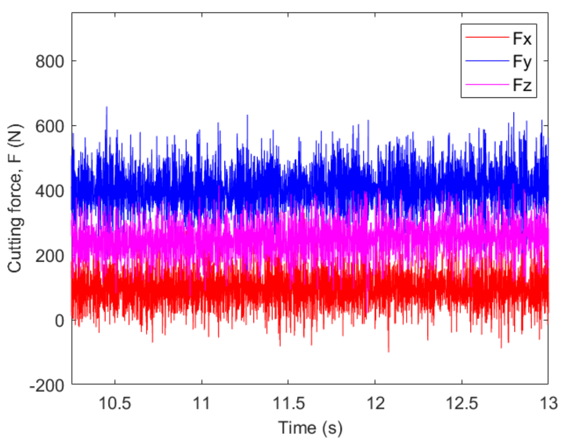

Fig. 11. Variation of the shear forces for:
Vs = 175 m/min, *d* = 1.25 mm, *f* = 0.25 mm/rev

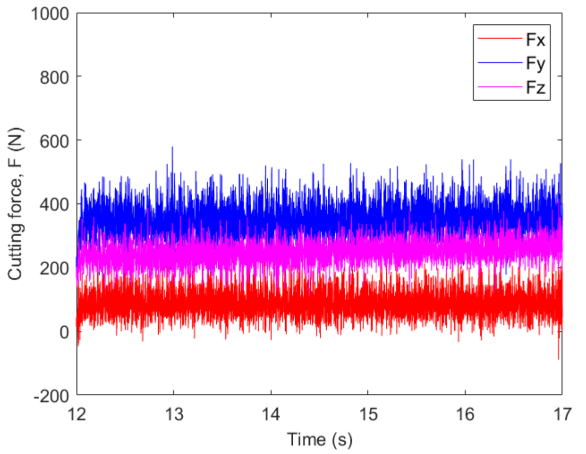

Fig. 12. Variation of the shear forces for:
Vs = 175 m/min, *d* = 1.25 mm, *f* = 0.2 mm/rev

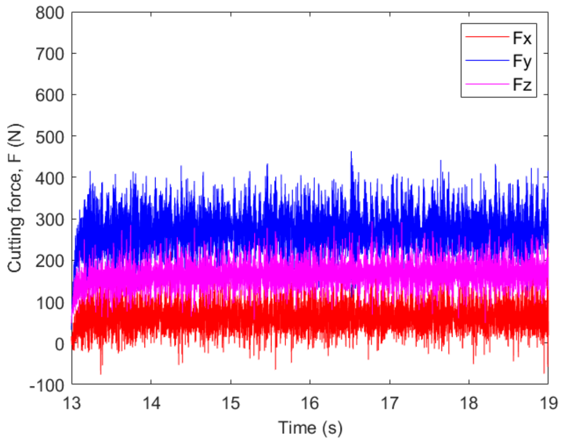

Fig. 13. Variation of the shear forces for:
Vs = 175 m/min, *d* = 1.25 mm, *f* = 0.15 mm/rev

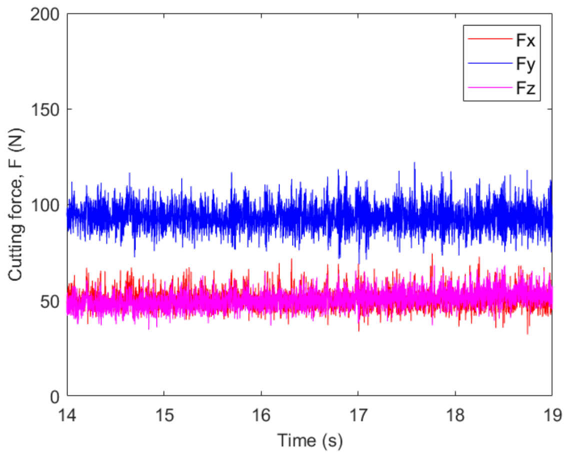

Fig. 14. Variation of the shear forces for:
Vs = 300 m/min, *d* = 0.5 mm, *f* = 0.15 mm/rev

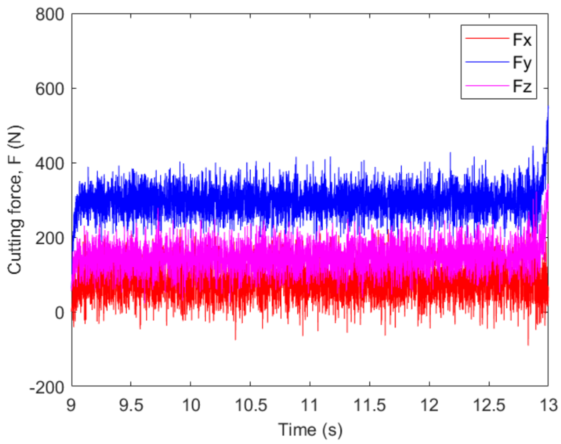

Fig. 15. Variation of the shear forces for:
Vs = 300 m/min, *d* = 1.25 mm, *f* = 0.2 mm/rev

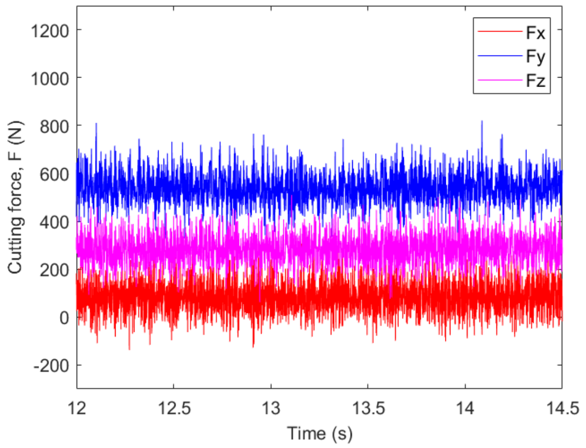

Fig. 16. Variation of the shear forces for:
Vs = 300 m/min, *d* = 2 mm, *f* = 0.25 mm/rev

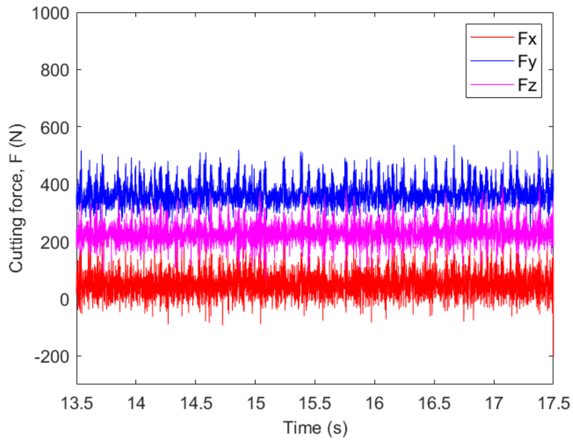

Fig. 17. Variation of the shear forces for:
Vs = 300 m/min, *d* = 2 mm, *f* = 0.15 mm/rev

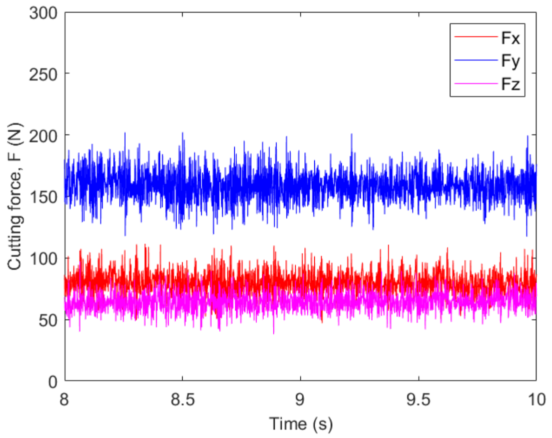

Fig. 18. Variation of the shear forces for:
Vs = 300 m/min, *d* = 0.5 mm, *f* = 0.25 mm/rev

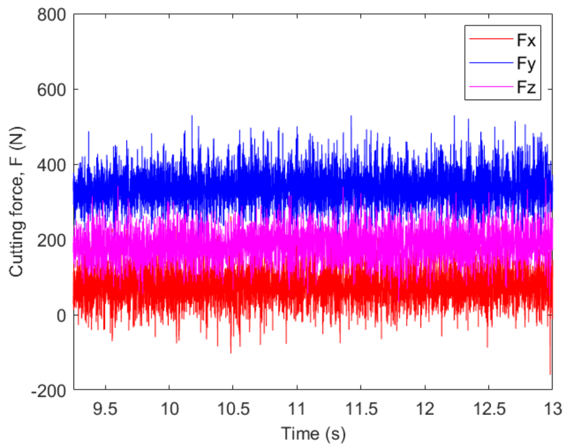

Fig. 19. Variation of the shear forces for:
Vs = 175 m/min, *d* = 1.25 mm, *f* = 0.2 mm/rev

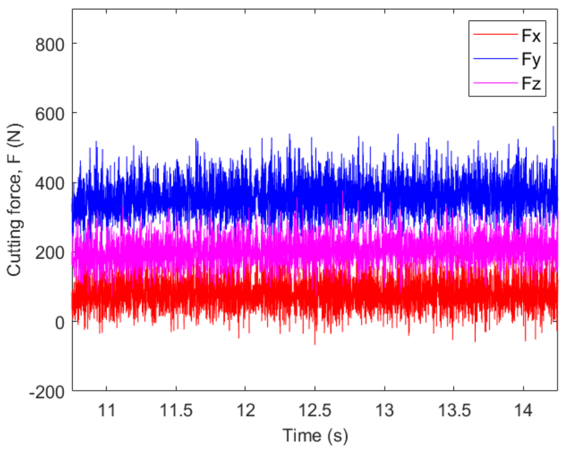

Fig. 20. Variation of the shear forces for:
Vs = 175 m/min, *d* = 1.25 mm, *f* = 0.2 mm/rev

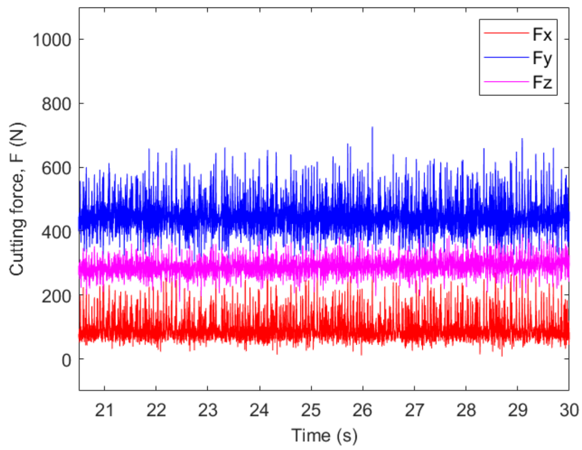

Fig. 21. Variation of the shear forces for:
Vs = 50 m/min, *d* = 1.25 mm, *f* = 0.2 mm/rev

For Run 1, the selected cutting parameters were a cutting speed of 50 m/min, a feed rate of 0.25 mm/rev, and a depth of cut of 0.5 mm. The cutting force components *Fx*, *Fy*, and *Fz* over time are presented in Figure 2. *Fz* exhibited the highest force values (450–500 N), followed by *Fy* (150–300 N), and *Fx* (100–200 N).

For Run 2, the designated cutting parameters were a cutting speed of 50 m/min, 0.25 mm/rev in case of feed rate and a depth of cut of 2.0 mm. The cutting force components *Fx*, *Fy*, and *Fz* over time are shown in Figure 3.

Based on the graph, *Fz* has the highest values, ranging from approximately 1250 to 1500 N. *Fy* falls in the intermediate range, approximately 500 to 1000 N. In contrast, *Fx* has the lowest values, ranging from around 0 to 250 N. In Run 3, the cutting parameters were set to a cutting speed of 50 m/min, a feed rate of 0.15 mm/rev and a depth of cut of 0.5 mm. The cutting force components *Fx*, *Fy*, and *Fz* over time are illustrated in Figure 4. As shown in the Figure 4, *Fz* recorded the highest force values, ranging from approximately 400 to 600 N. *Fy* displayed intermediate values, between 100 and 200 N, while *Fx* exhibited the lowest values, ranging from 0 to 100 N.

For Run 4, the selected cutting parameters included a cutting speed of 50 m/min, a feed rate of 0.15 mm/rev, and a depth of cut of 2.0 mm. The cutting force components *Fx*, *Fy*, and *Fz* over time are depicted in Figure 5. According to the graph, *Fz* exhibited the highest force values, ranging from approximately 600 to 1000 N. *Fy* displayed moderate values between 400 and 800 N, while *Fx* showed the lowest values, ranging from 0 to 200 N.

For Run 5, the cutting parameters were set to a cutting speed of 175 m/min, a feed rate of 0.2 mm/rev and a depth of cut of 2.0 mm. The cutting force components *Fx*, *Fy*, and *Fz* over time are illustrated in Figure 6. According to the graph, *Fy* recorded the highest force values, ranging from approximately 500 to 800 N. *Fz* exhibited intermediate values between 300 and 500 N, while *Fx* showed the lowest, ranging from 0 to 200 N.

For Run 6, the cutting speed was 175 m/min, with a feed rate of 0.25 mm/rev and a depth of cut of 1.25 mm. As shown in Figure 7, *Fy* again recorded the highest force, ranging from around 300 to 400 N. *Fz* followed, with values between 200 and 300 N, while *Fx* remained the lowest, ranging from 0 to 200 N.

For Run 7, the cutting parameters included a cutting speed of 175 m/min, a feed rate of 0.2 mm/rev and a depth of cut of 0.5 mm. The cutting force components *Fx*, *Fy*, and *Fz* over time are illustrated in Figure 8. According to the graph, *Fz* recorded the highest force values, ranging from approximately 140 to 200 N. *Fy* showed intermediate values, between 75 and 200 N, while *Fx* registered the lowest forces, ranging from 50 to 100 N.

For Run 8, the cutting speed remained at 175 m/min, with a feed rate of 0.15 mm/rev and a depth of cut of 1.25 mm. As shown in Figure 9, *Fy* exhibited the highest force values, ranging from about 150 to 400 N. *Fz* followed, with values between 150 and 250 N, and *Fx* recorded the lowest, ranging from 0 to 100 N.

For Run 9, the cutting parameters were set to a cutting speed of 175 m/min, a feed rate of 0.2 mm/rev and a depth of cut of 1.25 mm. The cutting force trends for *Fx*, *Fy*, and *Fz* over time are illustrated in Figure 10. As shown in the graph, *Fy* recorded the highest values, ranging from approximately 200 to 450 N. *Fz* displayed intermediate forces, between 200 and 300 N, while *Fx* showed the lowest, ranging from 0 to 200 N.

For Run 10, the cutting speed remained at 175 m/min, with an increased feed rate of 0.25 mm/rev and a constant depth of cut of 1.25 mm. As presented in Figure 11, *Fy* again exhibited the highest force, ranging from about 400 to 600 N. *Fz* followed with values between 200 and 400 N, and *Fx* remained the lowest, ranging from 0 to 200 N.

For Run 11, the parameters included a cutting speed of 175 m/min, a feed rate of 0.2 mm/rev and a depth of cut of 1.25 mm. The force data in Figure 12 show that *Fy* had the highest values, ranging from around 300 to 500 N. *Fz* fell in the intermediate range of 200 to 300 N, while *Fx* again registered the lowest force, between 0 and 200 N. For Run 12, the cutting parameters were set to a cutting speed of 175 m/min, a feed rate of 0.15 mm/rev and a depth of cut of 1.25 mm. The cutting force components *Fx*, *Fy*, and *Fz* over time are illustrated in Figure 13. According to the graph, *Fy* recorded the highest values, ranging from approximately 200 to 400 N. *Fz* exhibited intermediate values between 100 and 200 N, while *Fx* had the lowest, ranging from 0 to 100 N.

For Run 13, the cutting speed was increased to 300 m/min, with a feed rate of 0.15 mm/rev and a shallow depth of cut of 0.5 mm. As shown in Figure 14, *Fy* again recorded the highest cutting force, ranging from 70 to 100 N. In contrast, both *Fx* and *Fz* showed similar lower values, between 40 and 60 N.

For Run 14, the parameters included a cutting speed of 300 m/min, a feed rate of 0.2 mm/rev and a depth of cut of 1.25 mm. The force trends in Figure 15 reveal that *Fy* remained the dominant component, with values ranging from 200 to 400 N. *Fz* followed, with values between 100 and 200 N, and *Fx* showed the lowest forces, ranging from 0 to 100 N. In Run 15, the depth of cut was increased to 2.0 mm, the feed rate was raised to 0.25 mm/rev, and the cutting speed was kept at 300 m/min. The cutting force data in Figure 16 show *Fy* again having the highest values, ranging from 400 to 800 N. *Fz* came next, between 200 and 400 N, while *Fx* remained the lowest, ranging from 0 to 200 N. For Run 16, the cutting parameters were set to a speed of 300 m/min, a feed rate of 0.15 mm/rev and a depth of cut of 2.0 mm. As shown in Figure 17, *Fy* exhibited the highest cutting force, ranging from approximately 300 to 500 N. *Fz* showed moderate values between 200 and 300 N, while *Fx* recorded the lowest forces, ranging from 0 to 200 N.

For Run 17, the cutting speed was 300 m/min with a feed rate of 0.25 mm/rev and a depth of cut of 0.5 mm. According to Figure 18, *Fy* remained the dominant force, ranging from 150 to 200 N. *Fx* followed with values

between 75 and 100 N, while *Fz* showed the lowest readings, from 50 to 75 N.
For Run 18, the cutting parameters included a speed of 175 m/min, a feed rate of 0.2 mm/rev and a depth of cut of 1.25 mm. In Figure 19, *Fy* again recorded the highest values, ranging from 300 to 400 N. *Fz* showed intermediate values between 150 and 250 N, while *Fx* had the lowest forces, ranging from 0 to 175 N.
For Run 19, the same cutting parameters were maintained. As shown in Figure 20, *Fy* had the highest cutting force values, between 300 and 500 N. *Fz* ranged from 100 to 300 N, and *Fx* remained the lowest, from 0 to 150 N. For Run 20, the cutting speed was reduced to 50 m/min, with a feed rate of 0.2 mm/rev and a depth of cut of 1.25 mm. The cutting force data in Figure 21 shows *Fy* as the highest, ranging from 400 to 600 N. *Fz* followed with values between 200 and 400 N, while *Fx* showed the lowest forces, ranging from 0 to 200 N.

3.2. ANN Model Predictions

The MATLAB neural network toolbox was utilized, with data divided at 70% for training and 15% for testing and validation. For neural network model training, data was given in the form of input and target matrices. The network's training function is the backpropagation method with Levenberg-Marquardt (trainlm). The data separation technique used by Kalra and Kumar Gupta (2023) is the same as it was in their study. Additionally, Kalra and Kumar Gupta (2023) state that backpropagation neural network architecture is widely used type of neural network architecture and in process modeling.
Data separation, such as 70% for training, 15% for validation, and 15% for testing, is a well-established and widely used approach in machine learning. This division of data into distinct subsets serves a crucial purpose in building reliable and effective models. The 70% allocation for training provides the model with a substantial amount of data to learn from, which is essential for complex models or large datasets. A substantial training set allows the model to better grasp underlying patterns and correlations in the data, resulting in greater generalization and predictive capabilities. The 15% allocation for validation is also significant as it allows for a meaningful evaluation of the model during the hyper parameter tuning and model selection stages.
Although a larger validation set could provide more precise estimates of the model’s performance, a 15% split strikes a reasonable balance, ensuring enough data for evaluation without sacrificing training data. Similarly, the 15% allocation for testing is critical to assess the final model's generalization ability accurately. The test set should be representative of the real-world data that the model is likely to encounter in practical applications. By allocating 15% to testing, researchers can obtain an unbiased estimate of the model’s performance on independent and previously unseen examples. This ensures that the model’s reported performance is reliable and not influenced by any data it may have already seen during training or validation. Machine learning aims to build models that can generalize well to new, unseen data. The split helps achieve this goal by providing an appropriate amount of data for training, validation, and testing, thereby preventing overfitting and allowing the model to learn meaningful patterns.
Furthermore, to construct nonlinear interactions between independent and dependent parameters, the hyperbolic tangent sigmoid or tansig function was taken into consideration as a feature that activates each layer. Surface roughness was the output, and the inputs for the CNC turning process included cutting parameters (*Vs*, *f* and *d*). In the end, an ideal neural network structure was created by considering the statistical parameters of mean sum squared error (MSE) and average error (AE) between the target and predicted values.
Analyzing the mean squared error (MSE) and autoencoder (AE) of the training, testing, and total data sets allowed for the determination of the best neural network architecture. Different numbers of neurons and layers were used in the training, testing, and validation of various models, and the related errors were computed for each neuron.
Figures 22 to 25 compare MSE values for varying numbers of neurons in single and double hidden layers. The neural network with the lowest MSE (2.6857) across all data was a single hidden layer neural network with twelve neurons. In addition, in comparison to other neural network architectures, the AE values were discovered to be generally low across all data. Consequently, a neural network model with a 3-12-3 topology was used to predict surface roughness. Figure 26 shows a schematic illustration of the optimized ANN design.
The development of the ANN model underwent multiple iterations of training to prevent overtraining. The model’s performance was observed by calculating MSE and AE at various iterations. The results show that at 5000 iterations, the MSE and AE of the train and test and overall data were at their lowest. They then stayed relatively steady until 7000 iterations, at which point they abruptly increased to 8000 iterations. The corresponding AE values for the test and train data were 0.0004836, 0.0004836 and 0.3522 when the training was stopped after 20,000 iterations. Furthermore, the regression analysis for training, validation, test, and all data of the ANN model were shown in Figure 27, the values are 0.9960, 1, 0.9859, and 0.9943, respectively. All the values are approaching 1 which suggest a robust linear correlation between analysed variables.

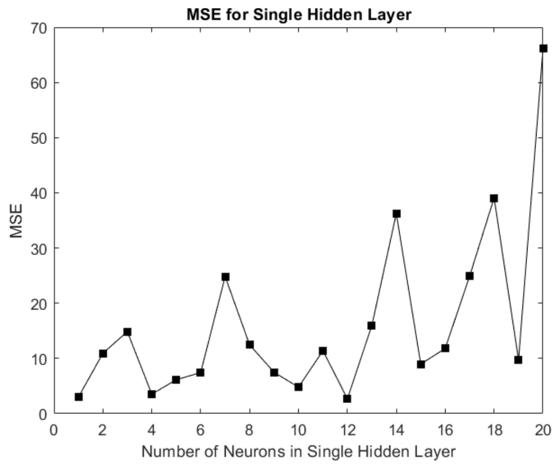

Fig. 22. MSE for SHL

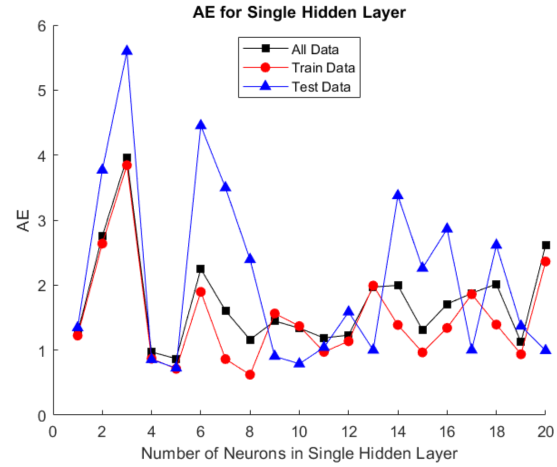

Fig. 23. AE for SHL

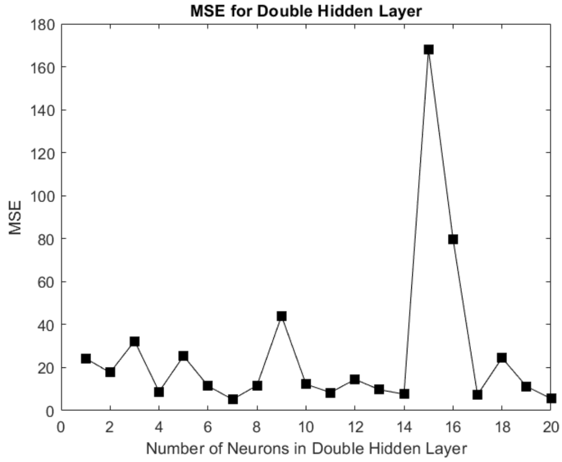

Fig. 24. MSE for DHL

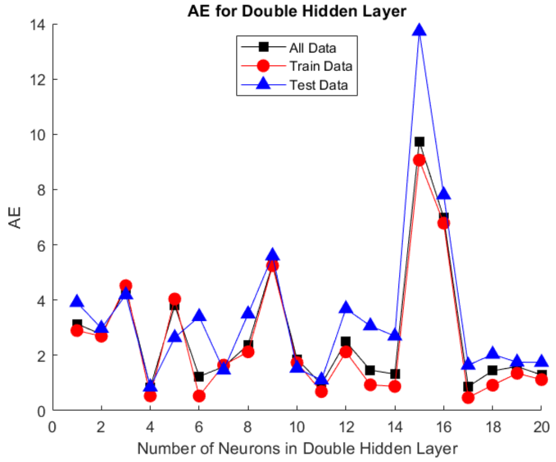

Fig. 25. AE for DHL

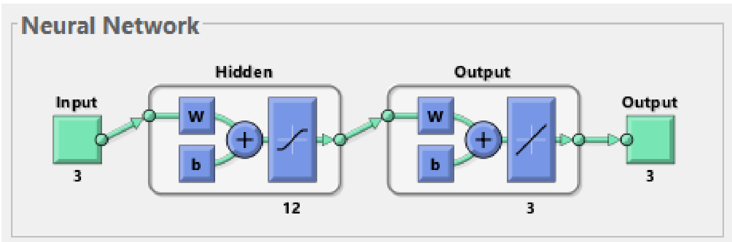

Fig. 26. Selected ANN architecture

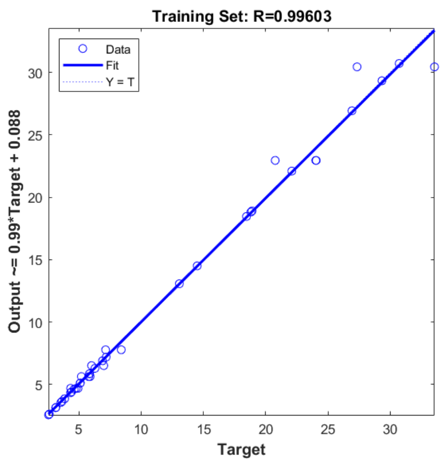

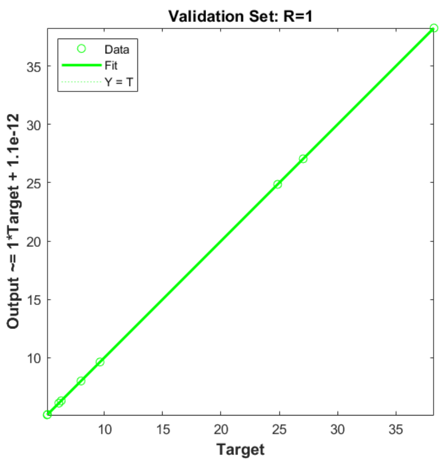

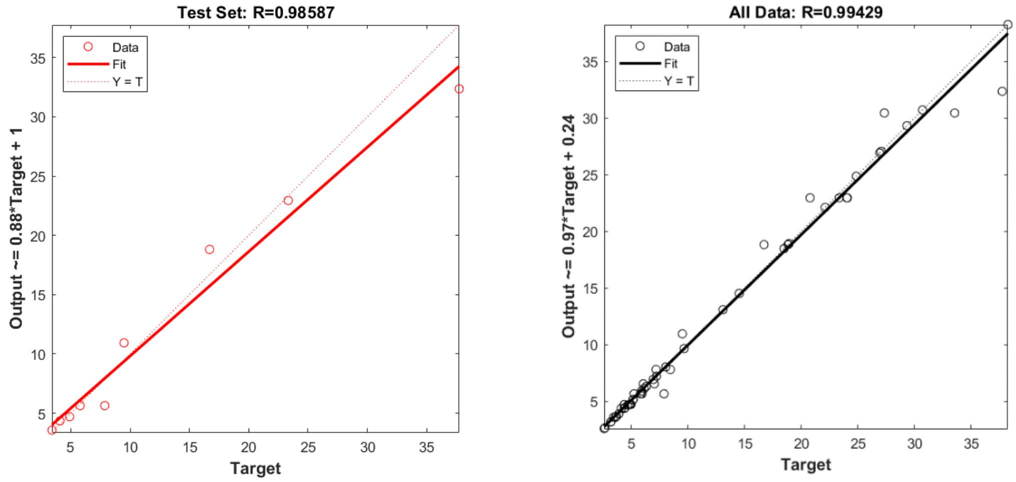

Fig. 27. Correlation between experimental results and predictions from the ANN model

3.3. RSM Model for Prediction

Using experimental data, an RSM model was developed to predict surface roughness in mild steel CNC turning. The three independent parameters and their interactions were represented by linear equations. The relationships between the input cutting speed, feed rate, and depth of cut are presented in Equations 1, 2, and 3, and the surface roughness measures *Ra* [µm], *Rq* [µm], and *Rz* [µm] are presented by the derived RSM model. Using well-established coefficients, the RSM model provides a precise mathematical relationship for predicting surface roughness. In this case, *A* stands for cutting speed, *Vs* [m/min]; *B* for feed rate *f* [mm/rev]; *C* for cut depth, *d* [mm].

$$Ra = 0.849434 - 0.007809A + 28.16437B - 1.11207C - 0.007419AB + 0.001564AC + 4.4855BC \quad (1)$$

$$Rq = 1.72111 - 0.011983A + 30.52272B - 1.26681C + 0.002049AB + 0.001708AC + 5.47117BC \quad (2)$$

$$Rz = 21.84992 - 0.077329A + 60.19777B - 10.48622C + 0.109488AB + 0.012117AC + 43.17667BC \quad (3)$$

Table 3 shows that the feed rate is the most important factor influencing Ra variation, with the biggest percentage contribution among the input factors. Surface roughness is affected by the following input factors: depth of cut (0.0004%), cutting speed (18.84%), and feed rate (70.76%). Additionally, Table 3 demonstrates that, with a p-value below 0.05, the feed rate is a highly significant characteristic. Thus, based on the ANOVA results, it can be said that a slight variation in the feed rate causes a notable variation in the Ra value. On the other hand, variations in the depth of cut barely make a difference.

Table 3. ANOVA results for *Ra*

Factors	df	Sum of Squares	Mean Square	F-value	p-value	PC (%)	Significance
A	1	8.42	8.42	25.94	0.0002	18.84	Important
B	1	31.63	31.63	97.52	< 0.0001	70.76	Very Important
C	1	0.0194	0.0194	0.0597	0.8108	0.0004	Not Important
AB	1	0.0172	0.0172	0.053	0.8215	0.0003	Not Important
AC	1	0.1719	0.1719	0.53	0.4795	0.3845	Not Important
BC	1	0.2263	0.2263	0.6978	0.4186	0.5062	Not Important
Residual	13	4.22	0.3244			9.441	Not Important
Total	19	44.70				100	

Table 4 shows that the feed rate is the most important factor influencing Rq variation, with the biggest percentage contribution among the input parameters. Surface roughness is affected by the following input factors: depth of cut (0.1416%), cutting speed (21.96%), and feed rate (67.32%). Additionally, Table 4 demonstrates that, with a p-value below 0.05, the feed rate is a highly significant characteristic. Therefore, the ANOVA results suggest that even a small change in the feed rate leads to a significant difference in the *Rq* value, whereas changes in the depth of cut have a negligible effect.

Table 4. ANOVA results for *Rq*.

Factors	df	Sum of Squares	Mean Square	F-value	p-value	PC (%)	Significance
A	1	13.92	13.92	29.34	0.0001	21.96	Important
B	1	42.68	42.68	89.99	< 0.0001	67.32	Very Important
C	1	0.0898	0.0898	0.1893	0.6706	0.1416	Not Important
AB	1	0.0013	0.0013	0.0028	0.9589	0.0021	Not Important
AC	1	0.2051	0.2051	0.4325	0.5223	0.3235	Not Important
BC	1	0.3368	0.3368	0.71	0.4147	0.5312	Not Important
Residual	13	6.17	0.4743			9.732	Not Important
Total	19	63.4				100	

As presented in Table 5, the feed rate exhibits the highest percentage contribution among the input parameters, making it the most significant factor affecting *Rz* variation. The contributions of the input parameters to surface roughness are as follows: feed rate (56.64%), cutting speed (26.92%), and depth of cut (0.0434%). Additionally, Table 5 indicates that the feed rate is a statistically significant parameter, with a p-value less than 0.05. Hence, the ANOVA results confirm that even a slight change in the feed rate can lead to a considerable variation in the *Rz* value, while changes in the depth of cut have a minimal impact.

Table 5. ANOVA results for *Rz*.

Factors	df	Sum of Squares	Mean Square	F-value	p-value	PC (%)	Significance
A	1	253.57	253.57	27.59	0.0002	26.92	Important
B	1	533.3	533.3	58.02	< 0.0001	56.64	Very Important
C	1	0.4088	0.4088	0.0445	0.8362	0.0434	Not Important
AB	1	3.75	3.75	0.4076	0.5343	0.3982	Not Important
AC	1	10.32	10.32	1.12	0.3085	1.096	Not Important
BC	1	20.97	20.97	2.28	0.1548	2.227	Not Important
Residual	13	119.48	9.19			12.69	Not Important
Total	19	941.81				100	

The feed rate is the most influential input parameter affecting fluctuations in *Ra*, *Rz*, and *Rq*, as indicated by its highest percentage contribution among the cutting parameters. Surface roughness is regulated by the following input factors: feed rate (56.64%), cutting speed (22.92%), and depth of cut (0.0434%). Additionally, the feed rate's p-value is less than 0.05, indicating statistical significance. The ANOVA results showed that while adjustments in the depth of cut had minimal effect, even small changes in feed rate significantly altered the Rz value. Figure 28 illustrates the variation in surface roughness values (*Ra*, *Rq*, and *Rz*) across different CNC turning process parameters. The surface plot shows that variations in depth of cut and cutting speed have a minor effect on surface roughness. In contrast, changes in feed rate result in greater variability, with both increases and decreases in roughness depending on the conditions.

According to the RSM analysis, a depth of cut of 1.074 mm, a feed rate of 0.1526 mm/rev, and a cutting speed of 298.9 m/min are the most efficient parameter values for the CNC turning operation. It was discovered that these parameters were within the specified ranges of 50–300 m/min for cutting speed, 0.15–0.25 mm/rev for feed rate and 0.5–2 mm for depth of cut. An additional ideal set of parameters was also found by the RSM pattern search: a depth of cut of 0.5 mm, a feed rate of 0.15 mm/rev, and a cutting speed of 300 m/min.

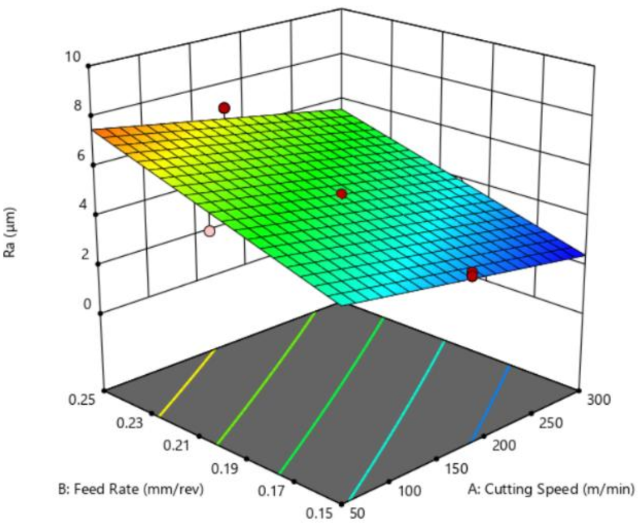
Ra (µm)
B: Feed Rate (mm/rev)
A: Cutting Speed (m/min)

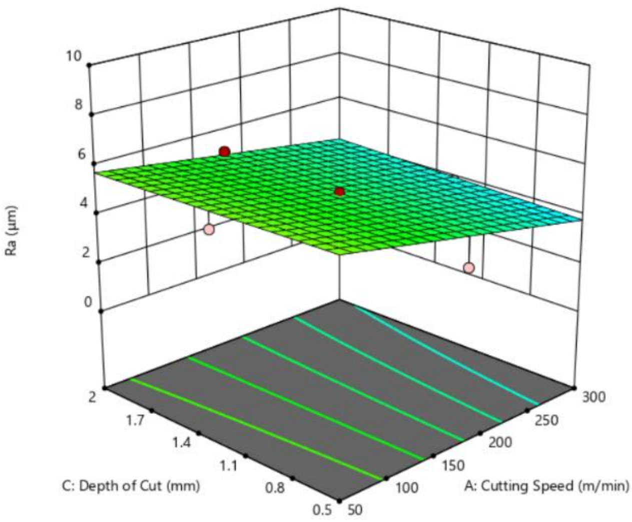
Ra (µm)
C: Depth of Cut (mm)
A: Cutting Speed (m/min)

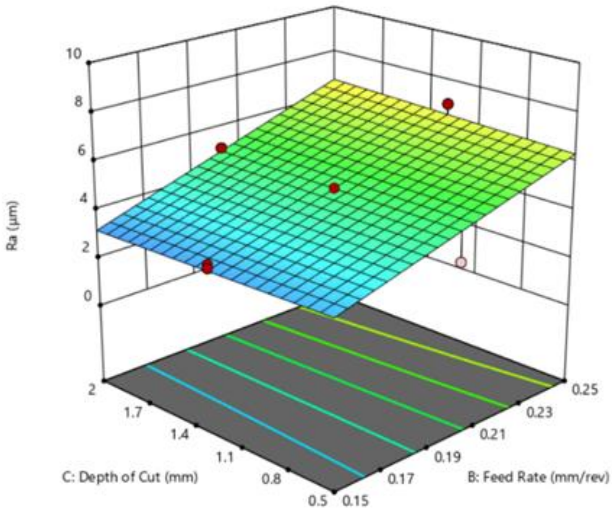
Ra (µm)
C: Depth of Cut (mm)
B: Feed Rate (mm/rev)

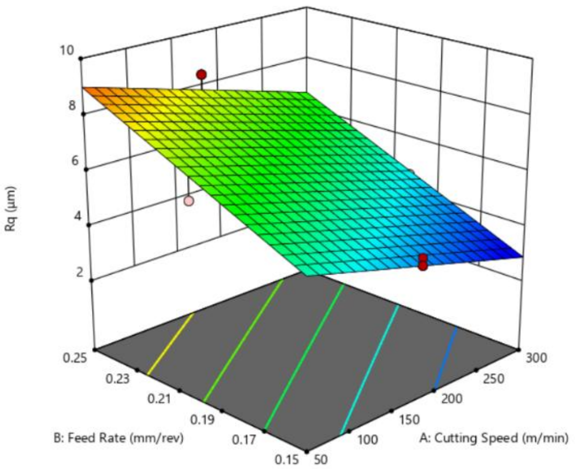
Rq (µm)
B: Feed Rate (mm/rev)
A: Cutting Speed (m/min)

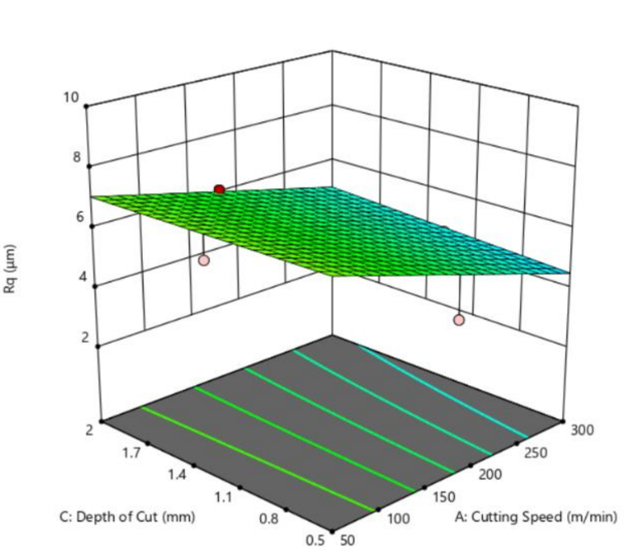
Rq (µm)
C: Depth of Cut (mm)
A: Cutting Speed (m/min)

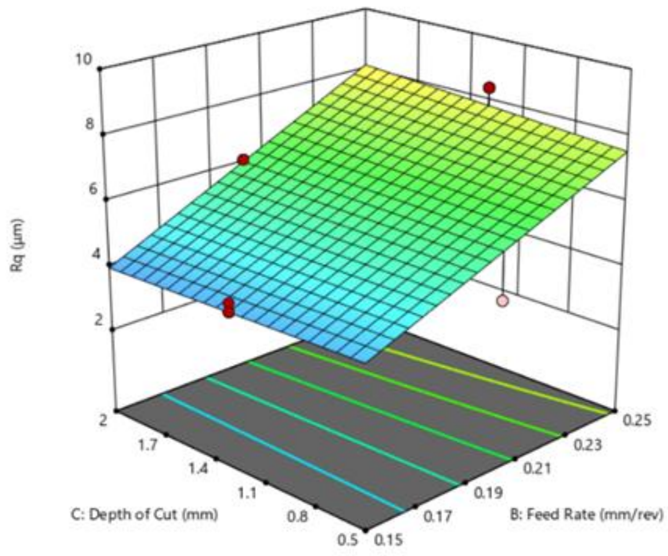
Rq (µm)
C: Depth of Cut (mm)
B: Feed Rate (mm/rev)

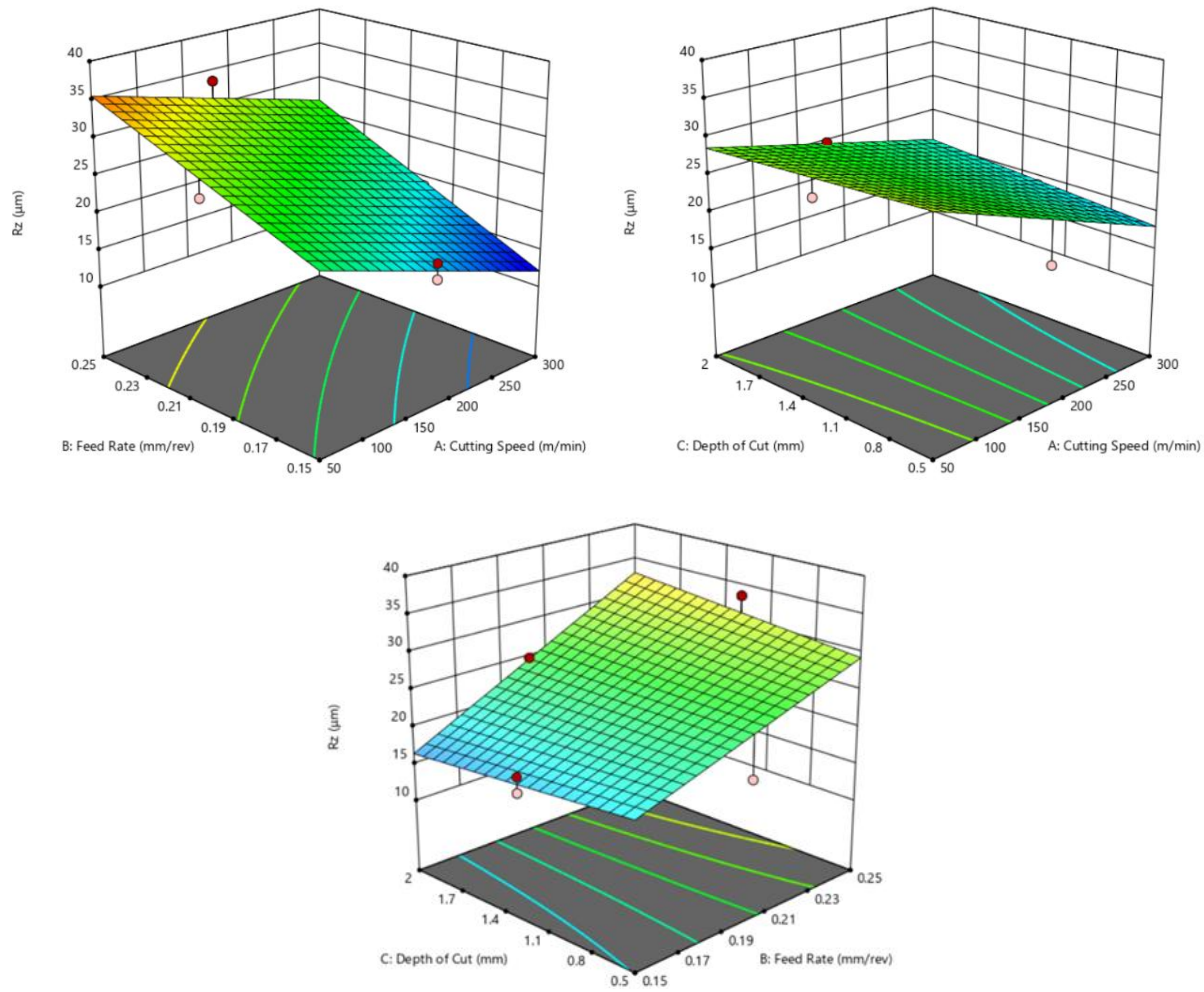

Fig. 28. Surface roughness *Ra*, *Rz*, and *Rq* are plotted in three dimensions in relation to CNC turning parameters

4. CONCLUSIONS

The investigation focused on the cutting variables: cutting speed (*Vs*), feed rate (*f*), and depth of cut (*d*). The results obtained from the analysis are summarized as follows:
The most crucial cutting parameter in CNC turning is feed rate (*f*), which is followed in order by cutting speed (*Vs*) and depth of cut (*d*).
Given the range values of 50 to 300 m/min, 0.15 to 0.25 mm/rev and 0.5 to 2 mm for *Vs*, *f* and *d* respectively. The RSM-pattern search gives the optimal values of 300 m/min for cutting speed, 0.15 mm/rev for feed rate, and 0.5 mm for depth of cut.
A comparison was made between the predictive accuracy of statistical and statistical machine learning techniques of RSM models. The RSM model had the lowest MAPE difference between the predictions and actual models, with 0.562, 0.514 and 0.654 for *Ra*, *Rq*, and *Rz*, respectively. The ANN model came in second, with 9.47%, 10.80%, and 9.97%.
The high R-value of 99.43% for the ANN model indicates a high degree of correlation between the experimental and predicted outcomes.

Author contributions: R. Samin: review and editing; initial draft writing; conceptualization; data curation; investigation; methodology; project administration; resources; supervision; validation; visualization; funding acquisition. **L. H. Noorazlan**: review and editing; initial draft writing; investigation; methodology; formal analysis. **M. I. S. Ismail**: methodology; investigation; validation; visualization. **M. H. Sulaiman**: resourses;

methodology; investigation; validation; visualization.
Funding source: The authors would like to thank Universiti Putra Malaysia for their support and research grant (GP/2017/9564400).
Conflicts of interest: There is no conflict of interest.
Acknowledgements: The authors would like to acknowledge the Department of Mechanical and Manufacturing Engineering in the Engineering Faculty, Universiti Putra Malaysia, for their collaboration in granting access to the laboratory

5. REFERENCES

[1] Jeffrey J. A., Kumar S. S., Vaidyaa P., Nicho A., Chrish A., Joshith J. (2022). *Effect of turning parameters in cylindricity and circularity for o1 steel using ANN*. Materials Today: Proceedings, 59, 1291-1294, https://doi.org/10.1016/j.matpr.2021.11.518

[2] Arunnath A., Masooth P.H.S. (2020). *Optimization of process parameters in CNC turning process on machining SCM440 steel by uncoated carbide and TiCN/Al2O3/TiN coated carbide tool under dry conditions*. Materials Today: Proceedings, 45, 6253–6269, https://doi.org/10.1016/j.matpr.2020.10.699

[3] Dhanaraj P. S., Rathinasuriyan C. (2022). *Optimization of fiber laser welding parameters for high strength aluminium alloy AA7075-T6*. Materials Today: Proceedings, 52, 283–289, https://doi.org/10.1016/j.matpr.2021.08.276

[4] Gopal M. (2020). *Prediction of surface roughness in turning of duplex stainless steel (DSS) using response surface methodology (RSM) and artificial neural network (ANN)*. Materials Today: Proceedings, 47, 6704–6711, https://doi.org/10.1016/j.matpr.2021.05.118

[5] Kalra G., Kumar G. A. (2023). *Mathematical modeling to estimate machining time during milling of Inconel 718 workpiece using ANN*. Materials Today: Proceedings, 78, 546–554, https://doi.org/10.1016/j.matpr.2022.11.314

[6] Kanaujia N., Behera J. K., Mohapatra S. K., Behera A., Jha, P., Joshi K. K., Routara B. C. (2022). *Process parameters optimization in CNC turning of aluminum 7075 alloy using TOPSIS method coupled with Taguchi philosophy*. Materials Today: Proceedings, 56, 989-994, https://doi.org/10.1016/j.matpr.2022.03.226

[7] Karakoç E., Çakır O. (2023). *Examination of surface roughness values of 6061-T6 aluminum material after machining and after anodizing process*. Materials Today: Proceedings, 80, 32-39, https://doi.org/10.1016/j.matpr.2022.10.058

[8] Karthikeyan S., Subbarayan M. R., Mathan Kumar P., Sivakandhan, C. (2022). *Computer vision-based surface roughness measurement using artificial neural network*. Materials Today: Proceedings, 60, 1325-1328, https://doi.org/10.1016/j.matpr.2021.09.314

[9] Kechagias J. D., Aslani K. E., Fountas N. A., Vaxevanidis N. M., Manolakos D. E. (2020). *A comparative investigation of Taguchi and full factorial design for machinability prediction in turning of a titanium alloy*. Measurement, 151, 107213, 1-13, https://doi.org/10.1016/j.measurement.2019.107213

[10] Korkmaz M. E., Yaşar N., Günay M. (2020). *Numerical and experimental investigation of cutting forces in turning of Nimonic 80A superalloy*. Engineering Science and Technology, an International Journal, 23(3), 664–673, https://doi.org/10.1016/j.jestch.2020.02.001

[11] Kumar S., Singh B. (2018). *Prediction of tool chatter in turning using RSM and ANN*. In Materials Today: Proceedings (Vol. 5). 2214-7853, https://doi.org/10.1016/j.matpr.2018.10.172

[12] Maier M., Kunstmann H., Zwicker R., Rupenyan A., Wegener K. (2022). *Autonomous and data-efficient optimization of turning processes using expert knowledge and transfer learning*. Journal of Materials Processing Technology, 303, 117540, 1-12, https://doi.org/10.1016/j.jmatprotec.2022.117540

[13] Merimi C., Hammouti B., Zaidi K., Elmsellem H. (2023). *Comparative study of inhibitory efficacy of drug (Acetaminophen) in 1 M HCl medium applied to carbon and mild steels*. Materials Today: Proceedings, 72, 3890-3895, https://doi.org/10.1016/j.matpr.2022.10.214

[14] Panwar V., Kumar Sharma D., Pradeep Kumar K. V., Jain A., Thakar C. (2020). *Experimental investigations and optimization of surface roughness in turning of en 36 alloy steel using response surface methodology and genetic algorithm*. Materials Today: Proceedings, 46, 6474–6481, https://doi.org/10.1016/j.matpr.2021.03.642

[15] Patel R., Patel S., Patel P., Parmar P., Vohra J. (2021). *Optimization of machining parameters for EN8D carbon steel by Taguchi's orthogonal array experiments in CNC turning*. Materials Today: Proceedings, 44, 2325–2329, https://doi.org/10.1016/j.matpr.2020.12.409

[16] Patnaik L., Maity S. R., Kumar S. (2021). *Modeling of wear parameters and multi-criteria optimization by Box-Behnken design of AlCrN thin film against gamma-irradiated Ti6Al4V counterbody*. Ceramics

International, 47(14), 20494–20511. https://doi.org/10.1016/j.ceramint.2021.04.059
[17] Paturi U. M. R., Cheruku S., Pasunuri V. P. K., Salike S., Reddy N. S., Cheruku S. (2021). *Machine learning and statistical approach in modeling and optimization of surface roughness in wire electrical discharge machining*. Machine Learning with Applications, 6 (2021) 100099, 1-11. https://doi.org/10.1016/j.mlwa.2021.100099
[18] Santhosh A. J., Tura A. D., Jiregna I. T., Gemechu W. F., Ashok N., Ponnusamy M. (2021). *Optimization of CNC turning parameters using face centred CCD approach in RSM and ANN-genetic algorithm for AISI 4340 alloy steel*. Results in Engineering, 11, (2021) 100251, 1-9, https://doi.org/10.1016/j.rineng.2021.100251
[19] Singh S., Singh S., Farwaha H. S., Grewal J. S., Ranjan N. (2022). *Investigation and development of aluminium matrix composite reinforced with silicon carbide using process of stir casting*. Materials Today: Proceedings. https://doi.org/10.1016/j.matpr.2022.11.124.
[20] Siva Surya M. (2022). *Optimization of turning parameters while turning Ti-6Al-4V titanium alloy for surface roughness and material removal rate using response surface methodology*. Materials Today: Proceedings, 62, 3479–3484. https://doi.org/10.1016/j.matpr.2022.04.300
[21] Soori M., Arezoo B., Dastres R. (2023). *Machine learning and artificial intelligence in CNC machine tools, A review*. Sustainable Manufacturing and Service Economics, 100009, 1-12. https://doi.org/10.1016/j.smse.2023.100009
[22] Soundhar A., Zubar H. A., Sultan, M. T. B. H. H., Kandasamy, J. (2019). *Dataset on optimization of EDM machining parameters by using central composite design*. *Data in brief*, *23*, 103671, 1-11. https://doi.org/10.1016/j.dib.2019.01.019
[23] Veeranaath V., Nandana Mohanty M., Kumar A., Kumar P. (2022). *ANN modeling of the significance of constraints in turning superalloys using coated PCBN tools*. Materials Today: Proceedings, 65, 20–28. https://doi.org/10.1016/j.matpr.2022.03.559
[24] Gopal M. (2020). *Optimization of machining parameters on temperature rise in CNC turning process of aluminium–6061 using RSM and genetic algorithm*. Int. J. Mod. Manuf. Technol, 12, 36-43.

Received: January 20th, 2025 / Accepted: June 15th, 2025 / Paper available online: June 20th, 2025